View metadata, citation and similar papers at core.ac.uk

brought to you by CORE

provided by Elsevier - Publisher Connector

International Journal of Solids and Structures 46 (2009) 1095–1104

Contents lists available at ScienceDirect

International Journal of Solids and Structures

journal homepage: www.elsevier.com/locate/ijsolstr

Comparison between Berkovich, Vickers and conical indentation tests: A three-dimensional numerical simulation study

N.A. Sakharova [a], J.V. Fernandes [a], J.M. Antunes [a,b,*], M.C. Oliveira [a]

[a] CEMUC – Department of Mechanical Engineering, University of Coimbra, Rua Luís Reis Santos, Pinhal de Marrocos, 3030-788 Coimbra, Portugal
[b] Escola Superior de Tecnologia de Abrantes, Instituto Politécnico de Tomar, Rua 17 de Agosto de 1808, 2200 Abrantes, Portugal

ARTICLE INFO

Article history:
Received 12 February 2008
Received in revised form 2 September 2008
Available online 12 November 2008

Keywords:
Numerical simulation
Indenter geometry

ABSTRACT

Three-dimensional numerical simulations of Berkovich, Vickers and conical indenter hardness tests were carried out to investigate the influence of indenter geometry on indentation test results of bulk and composite film/substrate materials. The strain distributions obtained from the three indenters tested were studied, in order to clarify the differences in the load–indentation depth curves and hardness values of both types of materials. For bulk materials, the differentiation between the results obtained with the three indenters is material sensitive. The indenter geometry shape factor, β, for evaluating Young's modulus for each indenter, was also estimated. Depending on the indenter geometry, distinct mechanical behaviours are observed for composite materials, which are related to the size of the indentation region in the film. The indentation depth at which the substrate starts to deform plastically is sensitive to indenter geometry.

© 2009 Published by Elsevier Ltd.

1. Introduction

Depth-sensing indentation tests are used to determine the hardness and the Young's modulus of bulk materials and thin films. Usually, Berkovich and Vickers indenters are used. Thus, the importance of understanding the relationship between the results of both indenters is obvious. In addition, the conical geometry is commonly used in bi-dimensional numerical simulation studies as equivalent to the Berkovich and Vickers indenters. Therefore, it is important to compare the results obtained using the three indenters.

To our knowledge, studies concerning the comparison of Berkovich, Vickers and conical indentation results are unusual. Only, a few experimental and numerical investigations (Rother et al., 1998; Min et al., 2004), concerning the equivalence of the results obtained from specific bulk materials, have been performed. Min et al. (2004) studied the influence of the geometrical shape of Berkovich, Vickers, Knoop and conical indenters on load–indentation depth curves and the strain field under the indentation for a copper specimen. However, the comparison of the indentation behaviour of bulk and composite materials with different indenter geometries still needs further investigation.

In the current study, three-dimensional numerical simulations of the indentation tests, in bulk and composite materials, were performed using the Berkovich, Vickers and conical indenters. Regarding bulk materials, a systematic study is presented which has a ratio between the residual indentation depth after unloading (h_f) and the indentation at the maximum load (h_{max}) in the range $0.20 < h_f/h_{max} < 0.98$. The geometrical correction factor needed to determine the Young's modulus, was also studied for the three indenters, for both bulk and composite materials. With regard to thin films, the study mainly focuses on the beginning of plastic deformation in the substrate, which defines the critical penetration depth above which the composite hardness results depend on the substrate's mechanical properties. The indentation test results, obtained using the three indenter geometries, are examined by comparing the load–indentation depth curves, the hardness values and the strain distributions in the indentation region.

2. Theoretical aspects

As mentioned above, depth-sensing indentation measurements are used to determine the hardness and the Young's modulus. The hardness, H_{IT}, is evaluated by (e.g., Oliver and Pharr, 1992)

$$H_{IT} = \frac{P}{A}, \tag{1}$$

where P is the maximum applied load and A is the contact area of the indentation, at the maximum load. The reduced Young's modulus, E_r, is determined from (e.g., Sneddon, 1965; Oliver and Pharr, 1992)

* Corresponding author. Address: CEMUC – Department of Mechanical Engineering, University of Coimbra, Rua Luís Reis Santos, Pinhal de Marrocos, 3030-788 Coimbra, Portugal. Tel.: +351 239 790700; fax: +351 239 790701.
E-mail address: jorge.antunes@dem.uc.pt (J.M. Antunes).

0020-7683/$ - see front matter © 2009 Published by Elsevier Ltd.
doi:10.1016/j.ijsolstr.2008.10.032

$$E_r = \frac{\sqrt{\pi}}{2\beta}\frac{1}{\sqrt{A}}\frac{1}{C}, \tag{2}$$

where β is the geometrical correction factor for the indenter geometry and C is the compliance. The specimen's Young's modulus, E_s, is obtained using the definition:

$$\frac{1}{E_r} = \frac{1-\nu_s^2}{E_s} + \frac{1-\nu_i^2}{E_i}, \tag{3}$$

where E and ν are the Young's modulus and the Poisson's ratio, respectively, of the specimen (s) and of the indenter (i). In this study, the indenter was considered rigid, and so $(1-\nu_i^2)/E_i = 0$.

The accuracy of the hardness and Young's modulus results, obtained with Eqs. (1)–(3), depends on the evaluation of contact area and compliance. In this study, the contact area, A, was evaluated using the contour of the indentation (see next section). Using this approach, contact area results are independent of the formation of pile-up and sink-in. The compliance C was evaluated by fitting the unloading part of the curve load–indentation depth, $(P-h)$, using the power law (Antunes et al., 2006)

$$P = P_0 + T(h-h_0)^m, \tag{4}$$

where T and m are constants obtained by fit and h_0 is the indentation depth which corresponds to a load value P_0, during unloading. In the fits, 70% of the unloading curve was used (Antunes et al., 2006).

Furthermore, another approach can be used for evaluating hardness and Young's modulus, allowing the Young's modulus to be obtained when the hardness is known, and *vice-versa*. This approach proposed by Joslin and Oliver (1990), uses the following equation, obtained by combining Eqs. (1) and (2)

$$\frac{P}{S^2} = \frac{\pi}{4\beta^2}\frac{H_{IT}}{E_r^2}. \tag{5}$$

The ratio between the maximum applied load (P) and the square of the stiffness ($S = 1/C$), P/S^2, is an experimentally measurable parameter that is independent of the contact area and so of the penetration depth (Joslin and Oliver, 1990). Moreover, if the hardness and the Young's modulus are known, the determination of the correction factor β is another useful application of Eq. (5).

3. Numerical simulation and materials

The numerical simulations of the hardness tests were performed using the HAFILM in-house code, which was developed to simulate processes involving large plastic deformations and rotations. This code considers the hardness tests a quasi-statistic process and makes use of a fully implicit algorithm of Newton–Rapson type (Menezes and Teodosiu, 2000). Hardness tests simulations can be performed using any type of indenter and take into account the friction between the indenter and the deformable body. A detailed description of the HAFILM simulation code has previously been given (Antunes et al., 2007).

Numerical simulations of the hardness tests were performed using Berkovich, Vickers and conical indenters. These three geometries are modelled with parametric Bézier surfaces, which allow a fine description of the indenter tip, namely an imperfection such as the one which occurs in the real geometry (Antunes et al., 2002). For ideal Berkovich, Vickers and conical indenter geometries with half-angles of 65.27°, 68° and 70.3°, respectively, the ratios between the projected area and the square of the indentation depth are equal to 24.5, for all cases. In this study, the three indenters, shown in Fig. 1, were modelled with tip imperfections, which consist in a plane normal to the indenters' axis. The Berkovich, Vickers and conical indenter tips have triangular, rectangular and circular shapes, respectively, and an area of approximately 0.0032 μm^2.

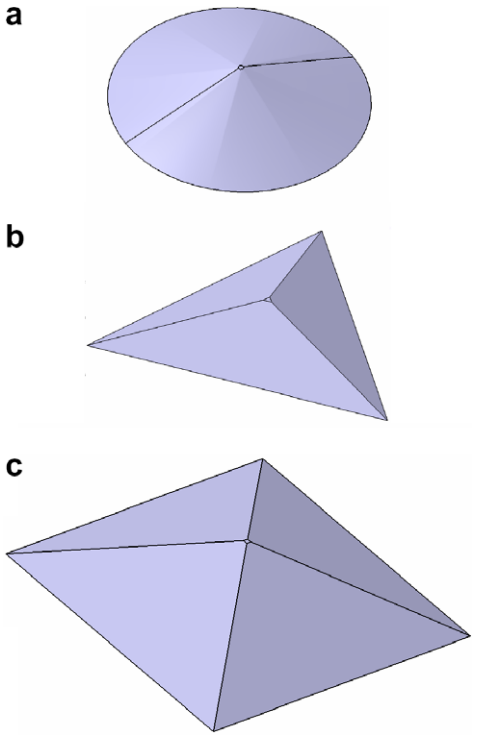

Fig. 1. Indenters geometry: (a) conical; (b) Berkovich; (c) Vickers.

This value corresponds to the imperfection usually observed in experimental Berkovich indenters (Antunes et al., 2007). Due to the imperfection at the tip, the area function of the indenters differs from the ideal. Table 1 presents the area functions of the indenters used in the numerical simulations. As can easily be seen, the three area function equations in this table represent equivalent evolutions of the area *versus* the indentation depth, in spite of their dissimilarity.

The test sample used in numerical simulations of bulk materials has both radius and thickness of 40 μm. It discretization was performed using three-linear eight-node isoparametric hexahedrons. The same sample was used in the simulation of the composite film/substrate materials. In those cases, a coating with a thickness equal to 0.5 μm (nine layers of elements in the film) was added. Due to geometrical and material symmetries in the $X = 0$ and $Z = 0$ planes, only a quarter of the sample was used in the numerical simulation of the Vickers and conical hardness tests. For the Berkovich simulation, only a symmetry condition in the $X = 0$ plane can be adopted. Thus, a half of the sample was used. In this context, the finite element meshes used in the numerical simulations with the Vickers and conical indenters were composed of 5832 elements for the bulk materials and 9072 for the thin films. In the case of the Berkovich simulations the number of elements was 11664 for the bulk materials and 18344 for the thin films. In all meshes the size of the finite elements in the indentation region was about 0.055 μm. The mesh refinement was chosen in order to provide accurate values of indentation contact area (Antunes et al., 2006).

Table 1
Area functions of the Vickers, Berkovich and conical indenters. The ideal indentation depth for the area A is: $h = \sqrt{A/24.5}$.

Indenter	Area function, A (μm^2)
Berkovich	$24.675h^2 + 0.562h + 0.003216$
Vickers	$24.561(h + 0.008)^2 + 0.206(h + 0.008)$
Conical	$24.5(h + 0.011427)^2$

At the maximum load, the contact area, A, was evaluated using geometrical considerations. For each contact node, the contact area is evaluated taking into account the contact status of its neighbouring nodes, as suggested by Tanner (1996), and also the normal distance between these nodes and the indenter; this guarantees the accurate estimation of the contact area (Oliveira, 2006; Oliveira et al., 2008). The error value for the contact area, and consequently for the hardness, was determined based on the comparison between the input and output values of the Young's modulus (Eq. (2)). The estimated hardness error is ±0.6%. Contact friction was considered between the indenter and the deformable body, with a Coulomb coefficient equal to 0.16 (Antunes et al., 2006).

Three-dimensional numerical simulations of the hardness tests for each indenter geometry were carried out on 22 bulk materials and nine composites, up to the same maximum indentation depth, $h_{max} = 0.3$ μm. The plastic behaviour of the materials used in the numerical simulations was modelled considering that the stress, σ and plastic strain, ε, relationship was described by the Swift law: $\sigma = k(\varepsilon + \varepsilon_0)^n$, where k, ε_0 and n (work-hardening coefficient) are material constants (the material yield stress is: $\sigma_y = k\varepsilon_0^n$). The constant ε_0 was considered to be 0.005 for all simulations. In bulk material modelling, three different work-hardening coefficients ($n = 0$, 0.25, 0.5) and two Young's moduli ($E = 200$ GPa and $E = 600$ GPa) were used. The Poisson's ratio, ν, was 0.3 for bulk and composite materials. In case of composite materials, the same work-hardening values of bulk materials were considered and the Young's modulus of the substrate and the film was 200 GPa, ($E_f/E_s = 1$). The H_f/H_s ratio between the hardness of the film (H_f) and substrate (H_s) was always higher than 2. The mechanical properties of bulk and composite materials used are presented in Tables 2 and 3, respectively.

4. Results and discussion

4.1. Bulk materials

4.1.1. Load–indentation depth curves and hardness

In this section, the load–indentation depth curves and hardness values obtained in the simulations using the three indenter geometries are compared, for the bulk materials of Table 2.

In a general way, the load–indentation depth curves are quite similar. However, small differences between curves can be easily observed when the h_f/h_{max} ratio decreases below about 0.65, whatever the work-hardening coefficient value of the material. It must be noted that the h_f/h_{max} parameter does not depend on the indentation depth for a given material (e.g., Bolshakov and Pharr, 1998) and is easily determined from the indentation curve. Moreover, it is well known that this ratio is related to the material properties, particularly the H_{IT}/E ratio between the hardness H_{IT} and the Young's modulus E. Fig. 2 shows two examples of load (P) *versus* indentation depth (h) curves obtained with Berkovich, Vickers and conical indenters, where h corresponds to the ideal indentation depth determined as indicated in Table 1. Fig. 1(a) and (b) correspond to materials with a work-hardening coefficient (n) of zero and a h_f/h_{max} ratio of to 0.74 (Fig. 1(a)) and 0.41 (Fig. 1(b)). The two other examples of load–indentation depth curves presented in Fig. 2 correspond to materials with work-hardening coefficient value of $n = 0.25$ and h_f/h_{max} equal to 0.88 (Fig. 2(c)) and 0.40 (Fig. 2(d)). For B3 and B14 materials ($h_f/h_{max} = 0.74$ and 0.88, respectively), the curves obtained are quite similar for all types of indenter tested. In the cases of B6 and B13 materials ($h_f/h_{max} = 0.41$ and 0.40), the curves obtained can be easily separated. Nevertheless, whatever the h_f/h_{max} value, the highest level of the curves corresponds to the one obtained with the Berkovich indenter and the lowest level to the one obtained with the conical indenter. Moreover, the difference between the Berkovich and the Vickers curves is higher than between the Vickers and the conical curves. Finally, it must be noted that similar results were obtained for materials having a work-hardening coefficient of $n = 0.5$.

Fig. 3 shows hardness values obtained in the indentation tests with Vickers, H^v, and conical, H^c, indenters normalized by the Berkovich indenter hardness, H^b, as a function of the ratio h_f/h_{max} (i.e., for bulk materials with different mechanical properties). As can be seen in Fig. 3, both ratios H^v/H^b and H^c/H^b are slightly lower than 1, whatever the value of the ratio h_f/h_{max}, which means that the hardness values for the Berkovich are always higher than those for the Vickers and conical indenters. Moreover, the H^v/H^b and H^c/H^b ratios decrease when h_f/h_{max} decreases. For values of h_f/h_{max} close to 1, the H^v/H^b and H^c/H^b ratios tend to approach 1, while for h_f/h_{max} values close to 0.2, the H^v/H^b and H^c/H^b ratios tend towards values close to 0.96 and 0.94, respectively. This is in agreement with the

Table 2
Mechanical properties of the bulk materials used in the numerical simulation. The hardness results, H^b, were obtained with the Berkovich indenter.

Material	Work-hardening coefficient, n	σ_y (GPa)	E (GPa)	H^b (GPa)	h_f/h_{max}
B1	≈0	1.00	200	3.90	0.92
B2		2.00		7.00	0.87
B3		5.00		13.67	0.74
B4		10.00		21.22	0.60
B5		15.00		26.43	0.50
B6		20.00		30.30	0.41
B7		12.05	600	34.93	0.78
B8	0.25	0.1	200	0.73	0.98
B9		0.25		1.93	0.96
B10		4.00		18.38	0.66
B11		6.00		23.33	0.55
B12		8.00		27.04	0.48
B13		10.00		29.91	0.40
B14		2.82	600	19.01	0.88
B15		16.41		66.48	0.57
B16	0.50	0.15	200	2.10	0.95
B17		0.25		3.49	0.94
B18		2.00		18.14	0.65
B19		4.00		26.56	0.46
B20		6.00		31.34	0.35
B21		25.32	600	104.62	0.25
B22		29.88		108.97	0.21

Table 3
Mechanical properties of the film, substrate and composite materials used in the numerical simulations. The hardness results, for the film, H_f^b, substrate, H_s^b and composite, H_c^b, were obtained with the Berkovich indenter. σ_y^f (σ_y^s) and n_f (n_s) are the yield stress and the work-hardening coefficient of the film (substrate), respectively.

Composite	σ_y^f (GPa)	n_f	σ_y^s (GPa)	n_s	H_f^b (GPa)	H_s^b (GPa)	H_f^b/H_s^b	H_c^b (GPa)
C1	20	≈0	2.00	≈0	30.30	7.00	4.33	23.15
C2			5.00		30.30	13.67	2.22	24.75
C3			0.25	0.50	30.30	3.49	8.67	24.29
C4	10	0.25	2.00	≈0	29.91	7.00	4.27	21.75
C5			5.00		29.91	13.67	2.19	24.49
C6			0.50	0.25	29.91	3.57	8.39	22.02
C7	6	0.50	2.00	≈0	31.34	7.00	4.48	22.61
C8			5.00		31.34	13.67	2.29	24.82
C9			0.25	0.50	31.34	3.49	8.97	22.51

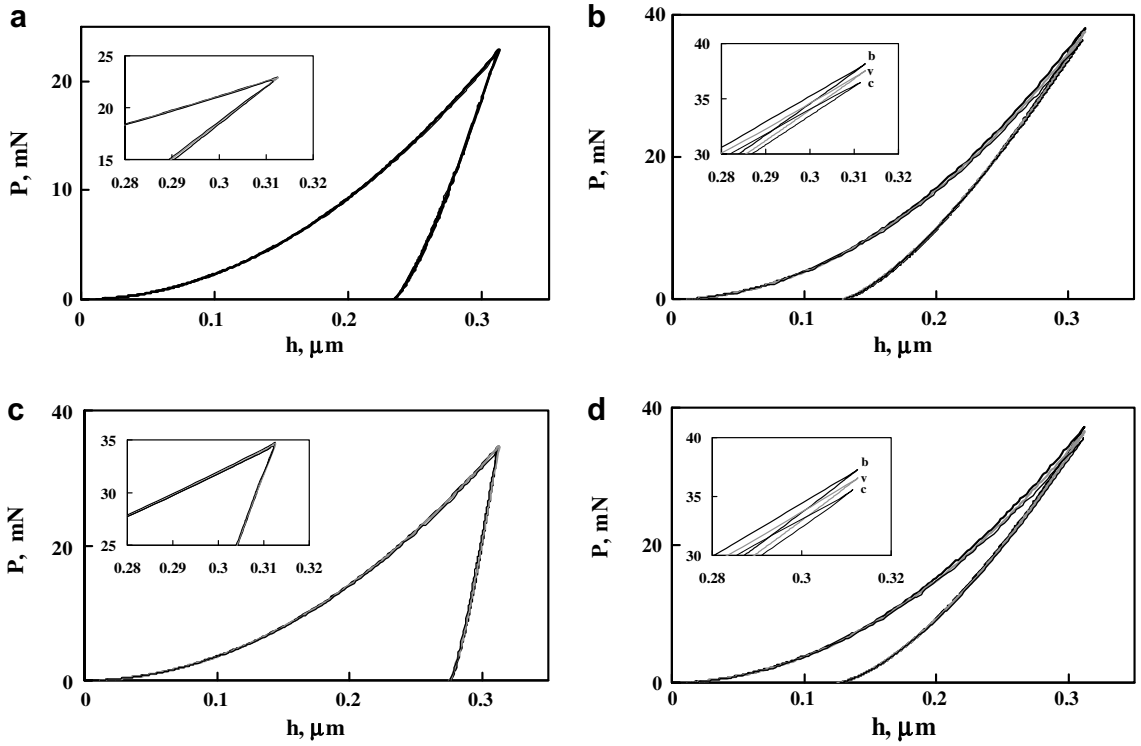

Fig. 2. Load–indentation depth curves for the materials: (a) B3 ($n = 0$ and $h_f/h_{max} = 0.74$); (b) B6 ($n = 0$ and $h_f/h_{max} = 0.41$); (c) B14 ($n = 0.25$ and $h_f/h_{max} = 0.88$); (d) B13 ($n = 0.25$ and $h_f/h_{max} = 0.40$). Indenters: b, Berkovich; v, Vickers; c, conical.

above discussed results concerning the load–indentation depth curves, which show higher differentiation between the curves obtained with the three indenter geometries, for lower h_f/h_{max} values than for higher ones. It must be mentioned that the most common materials show h_f/h_{max} values higher than 0.7, and so the H^v/H^b and H^c/H^b ratios are higher than 0.97 and 0.96, respectively.

4.1.2. Indenter tip imperfection

The tip imperfection of the indenter does not affect the hardness results, as discussed in this section. Actually, in a recent study, Antunes et al. (2007) concluded that a correction of the geometry of the Vickers indenters with offset, using the respective area function, is enough to obtain accurate values of the mechanical properties, namely the Young's modulus and the hardness. In this study, the modulation of the Vickers indenter was performed for five different sizes of offset, and the load–indentation depth curves become coincident after correction. Moreover, when the evolution of $k = P/h^2$ at each loading point (from Kick's law: $P = kh^2$, where P is the load and h is the indentation depth) was represented as function of the indentation depth for the different offset sizes, $k = P/h^2$ becomes constant and equal for all indenters, for high enough indentation values (depending on the size of the offset).

The geometrical imperfections of the indenters used in the present study were designed to make the numerical indenter as similar as possible to the experimental case. The size of the imperfection is equal to lowest tip imperfection size used in the previous study (an area of approximately 0.0032 μm^2 (Antunes et al., 2007)). In order to ensure that the estimation of the material hardness is not affected by indenter tip imperfections, the evolution of $k = P/h^2$, at each point of the loading part of the load–indentation depth curves (after correction with the area function), was represented as function of the indentation depth, for the three indenters used in current study. Fig. 4 shows two examples of this evolution. For indentation depths higher than 0.10 μm, the $k = P/h^2$ value becomes constant for each indenter. This means that the loading curves are self similar after this indentation depth. Moreover, for materials with high h_f/h_{max} values, the constant level is equal for the three indenters (see example of Fig. 4(a)), while for materials with low h_f/h_{max} values, this level can be easily separated, for the three indenters (Fig. 4(b)).

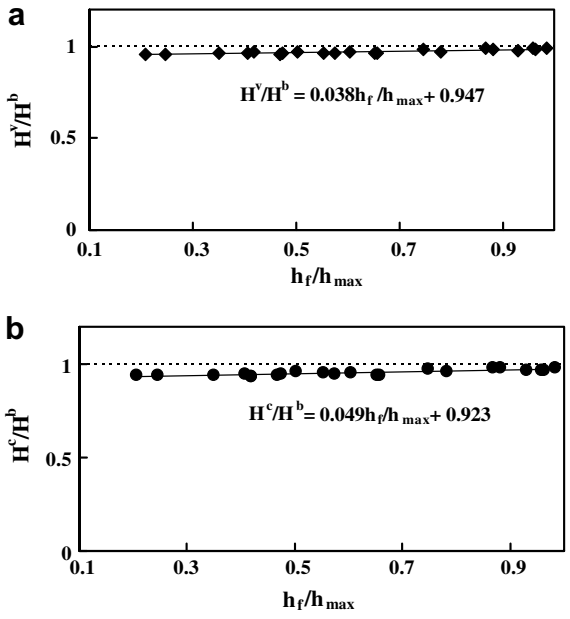

Fig. 3. Hardness results obtained for: (a) Vickers and (b) conical indenters. Both results are normalized by the hardness results obtained for the Berkovich indenter.

4.1.3. Strain distribution

Fig. 5 show the equivalent plastic strain distributions obtained at maximum load for the materials presented in Fig. 2(a) and (b). For B3 material, with $h_f/h_{max} = 0.74$ and $n = 0$, the maximum value of equivalent plastic strain is higher for the Berkovich indentation (≈0.549) than for Vickers (≈0.386) or conical (≈0.366) (Fig. 5 (left hand side)). For Berkovich indentation, the maximum plastic strain region is located just at the surface in the edge regions of the indentation (Fig. 5(a)); for Vickers indentation, the maximum plastic strain region is sited beneath the indentation surface as well as at the surface, in the edge region of the indentation (Fig. 5(b)); in the case of the conical indentation the maximum plastic strain region is located just under the surface (Fig. 5(c)). So, the presence of edges in the indenter geometry can influence the plastic strain under the indentation.

The case of low h_f/h_{max} value (material B6) is shown in Fig. 5 (right hand side). This material, with $h_f/h_{max} = 0.41$ and $n = 0$, also presents the maximum value of equivalent plastic strain for the Berkovich indenter (≈0.403), followed by the Vickers (≈0.366) and conical (≈0.362) ones (see the right hand side of Fig. 5(a–c), respectively). However, for this material, differences are more attenuated and the region with maximum equivalent plastic strain is located under the indentation surface, whatever the indentation geometry (for the Berkovich geometry only, high values of plastic strain occur in regions in contact with the surface, near the edge of the indentation (Fig. 5(a)). These results are qualitatively valid whatever the materials' work-hardening coefficient ($n = 0$ and also

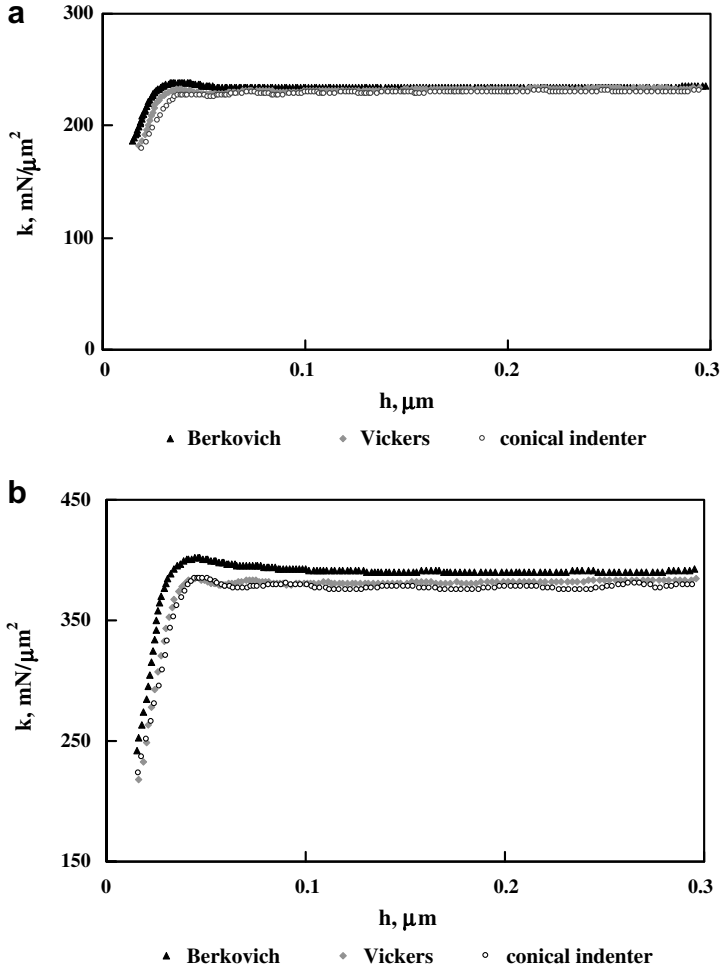

Fig. 4. Evolution of the value of the constant k as function of the indentation depth, obtained from the numerical simulation with Berkovich, Vickers and conical indenters: (a) B3 ($n = 0$ and $h_f/h_{max} = 0.74$); (b) B6 ($n = 0$ and $h_f/h_{max} = 0.41$).

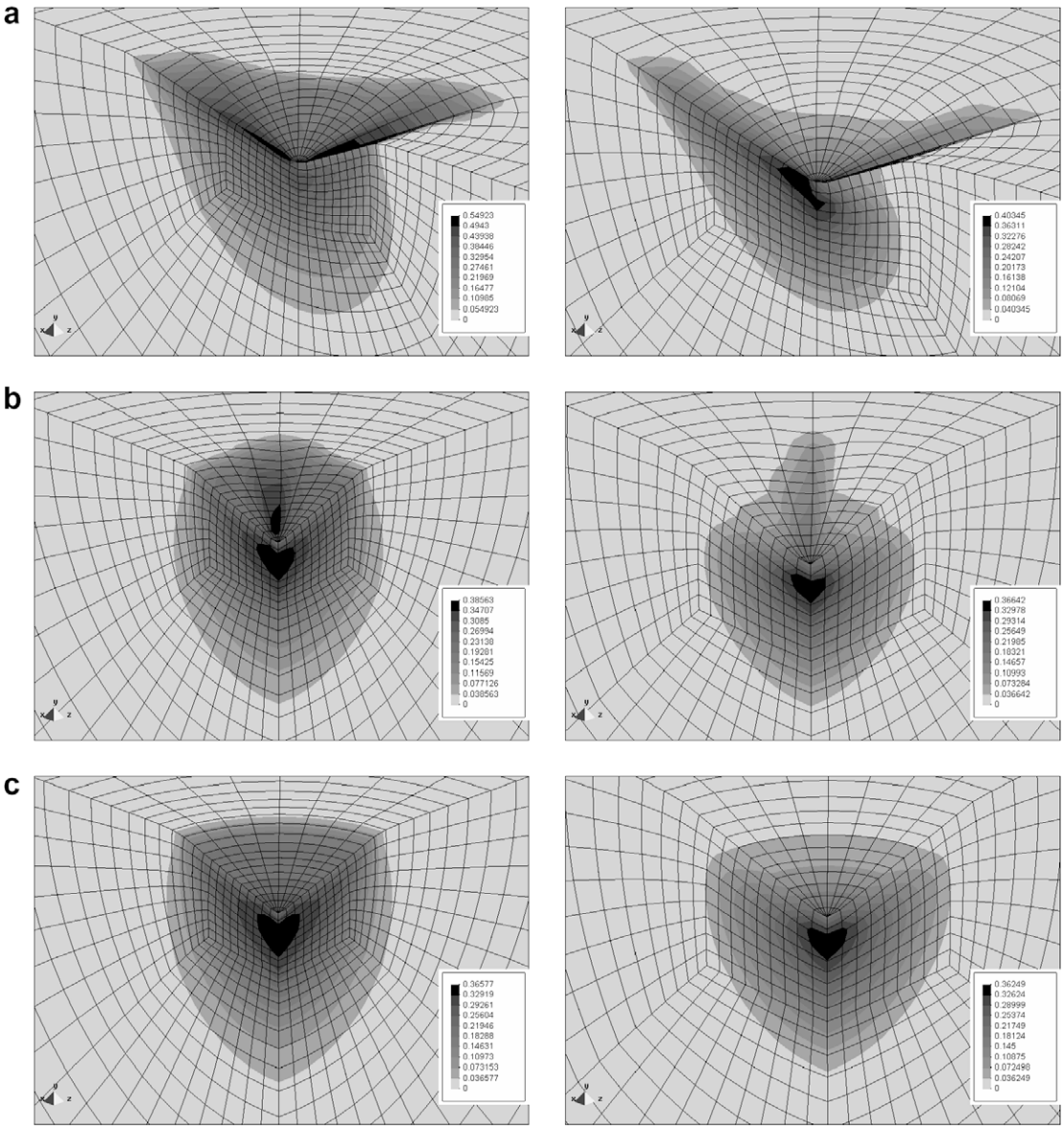

Fig. 5. Equivalent plastic strain distribution obtained at the maximum load for the materials B3 (left hand side) and B6 (right hand side) in numerical simulations with the indenters: (a) Berkovich; (b) Vickers; (c) conical.

for $n = 0.25$ and 0.5), which suggests that the higher differentiation between the load–indentation depth curves, observed when the h_f/h_{max} value decreases, is not related to differences in maximum equivalent plastic strain values. In fact, the differences between the maximum equivalent plastic strains observed using the three indenters are higher when the load–indentation depth curves are closer, i.e., when the h_f/h_{max} value approaches 1. Fig. 5 also shows that plastic strain distributions are dependent on the indentation geometry. The plastic strain region is less spherical and slightly less deep for the Berkovich indenter than for the Vickers and conical ones. This is the case in both materials but mainly for the material with $h_f/h_{max} = 0.41$. These differences in the plastic strain region's geometry, obtained with the three types of indenter, are probably the main reason why the load–indentation depth curves are not strictly identical.

4.1.4. Young's modulus

The Young's modulus of the bulk materials was evaluated considering the results obtained using the three types of indenter. Fig. 6 shows that the Young's modulus values, E_{eval}, are normalized by the value used as input in the numerical simulation, E_{input}, as a function of h_f/h_{max} (E_{eval} was determined using $\beta = 1$, in Eq. (2)). The ratio E_{eval}/E_{input} is quite constant and always higher than 1, whatever the indenter used. The correction factor β was estimated from the mean value of E_{eval}/E_{input}, for each indenter. The β values obtained were 1.081, 1.055 and 1.034 for the Berkovich (Fig. 6(a)), Vickers (Fig. 6(b)) and conical (Fig. 6(c)) indenters, respectively.

Eq. (5) was used in order to confirm the above correction factor β values. E_r was determined from Eq. (3) using the input Young's modulus, E_{input}, and the hardness values, H_{IT}, were determined using Eq. (1), where the contact area is evaluated directly from numerical simulation results. Fig. 7 shows, for the three indenter geometries, the ratio P/S^2 *versus* H_{IT}/E_r^2 obtained for the bulk materials. All the straight lines in Fig. 7 pass through the origin of the axes as indicated by Eq. (5) (all curves match for $H_{IT}/E_r^2 = 0$, i.e., for materials with rigid-plastic behaviour, which corresponds to the ratio $h_f/h_{max} = 1$). The β factor is evaluated from the slope, x, of the straight lines, related with β through $x = \pi/4\beta^2$. Fig. 6 gives

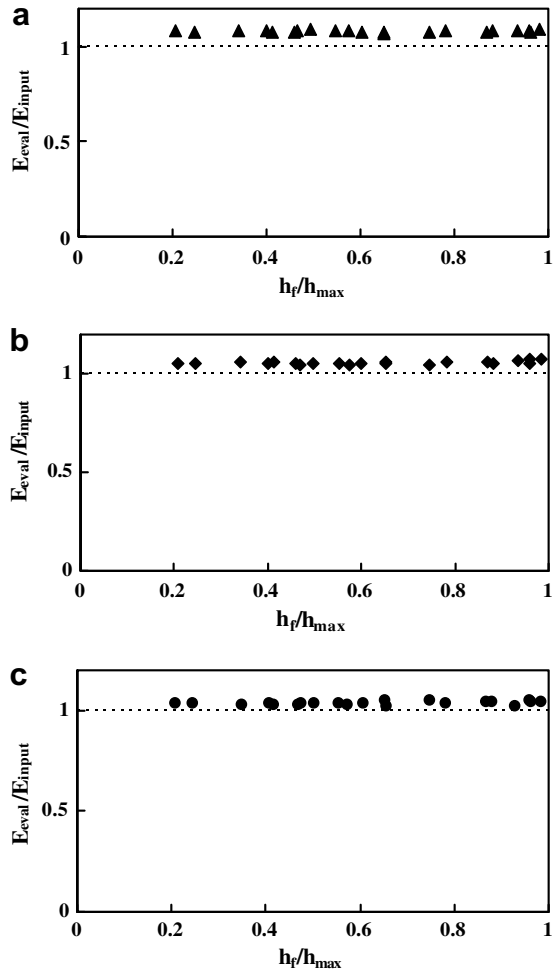

Fig. 6. Young's modulus results, E_{eval}, normalized by E_{input}, obtained for bulk the materials in numerical simulation with the indenters: (a) Berkovich; (b) Vickers; (c) conical.

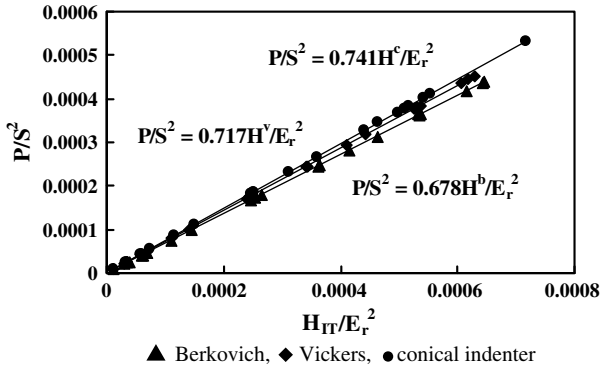

Fig. 7. Representation of the ratio P/S^2 *versus* H/E_r^2 of the bulk materials, for the three indenter geometry.

β factor values of 1.074, 1.045 and 1.029 for Berkovich, Vickers and conical indenters, respectively. These values are quite similar to the ones previously calculated from Fig. 6. In this context, it can be concluded that a β factor greater than 1 should be considered for the three indenters, when using Eq. (2) to determine the Young's modulus. Moreover, the β factor increases with deviation of the indenter's geometry from circular (conical indenter) to Vickers (four-sided pyramidal) and Berkovich (three-sided pyramidal). The same conclusion has been reached in several analytical and numerical studies (e.g., Antunes et al., 2006; Bolshakov and Pharr, 1998; Cheng and Cheng, 1999). However, these previous studies proposed a wide range of β values, which generate some uncertainty about the adequate values. For example, based on numerical simulation results, Dao et al. (2001) propose values for the β correction factor of to 1.096, 1.072 and 1.060 for the Berkovich, Vickers and conical indenters, respectively. In a recent three-dimensional numerical simulation study, using several materials with different Young's moduli and work-hardening coefficients, a β value of 1.05 was found for the case of the Vickers indenter (Antunes et al., 2006). Finally, is important to state that using the β values obtained in the current study, using the data presented in Fig. 7, the maximum error in the evaluation of the Young's modulus, in each individual simulation, was at about 1.4%, 1.8% and 1.7% for the Berkovich, Vickers and conical indenters, respectively.

4.2. Composite materials

Numerical simulations of composite materials concern cases where the hardness of the film H_f is higher than the hardness of the substrate H_s, as shown in Table 3. Load–indentation depth curves and strain distributions were studied to improve understanding of the influence of the indenter geometry on the composite's behaviour during indentation.

The load–indentation depth curves obtained from Berkovich, Vickers and conical indentation tests on composite materials are not coincident, and show a non-negligible difference, for the H_f/H_s values studied (where $H_f/H_s > 1$). Examples of such load–indentation depth curves are shown in Fig. 8, for three values of the ratio between the film (H_f) and the substrate (H_s) hardness (H_f/H_s of about 2.22, 4.33 and 8.67). Fig. 8 also shows the load–indentation depth curves of the corresponding film and substrate. It can be easily seen that the differences between the Berkovich, Vickers and conical indentation curves are higher for the composite than for the respective film and substrate. The Berkovich indentation curve is higher than the Vickers, which in turn is higher than the conical, as for bulk materials. In addition, the numerical study of the composite materials' hardness revealed that, for all the composites in Table 3, the H_c^v/H_c^b ratio between the Vickers and the Berkovich hardness and the H_c^c/H_c^b ratio between the conical and the Berkovich hardness are always lower than 1. This means that the hardness obtained with the Berkovich indenter is always higher than with the Vickers and conical indenters, the same as for the bulk materials. However, the observed differences are higher for composite than for bulk materials. In fact, for the composite materials studied, the ratio H_c^v/H_c^b is in the range 0.88 to 0.96, and decreases when the ratio H_f/H_s increases, as shown in Fig. 9, whatever the work-hardening coefficient values of the film and the substrate. In this figure, only the ratio H_c^v/H_c^b is shown, for simplification.

In order to understand such differences between the behaviour of composite materials under Berkovich, Vickers and conical indentation tests, strain distribution at low indentation depths in the composite was studied. The C2 composite material is taken as an example. For a penetration depth of 0.15 μm, the substrate is more deformed in the case of the Vickers and conical indenters than in the case of the Berkovich indenter, as shown in Fig. 10. The indentation depths at which the substrate starts to deform plastically were also determined for all three indenters tested. The plastic response of substrate material begins earlier for conical and Vickers indenters, at penetration depths of 0.127 and 0.129 μm, respectively. For the Berkovich indenter the plastic deformation of the substrate occurs for a penetration depth value of 0.137 μm. The correspondent equivalent plastic strain distributions are represented in Fig. 11 and confirm the delayed plastic response of the substrate in the Berkovich case.

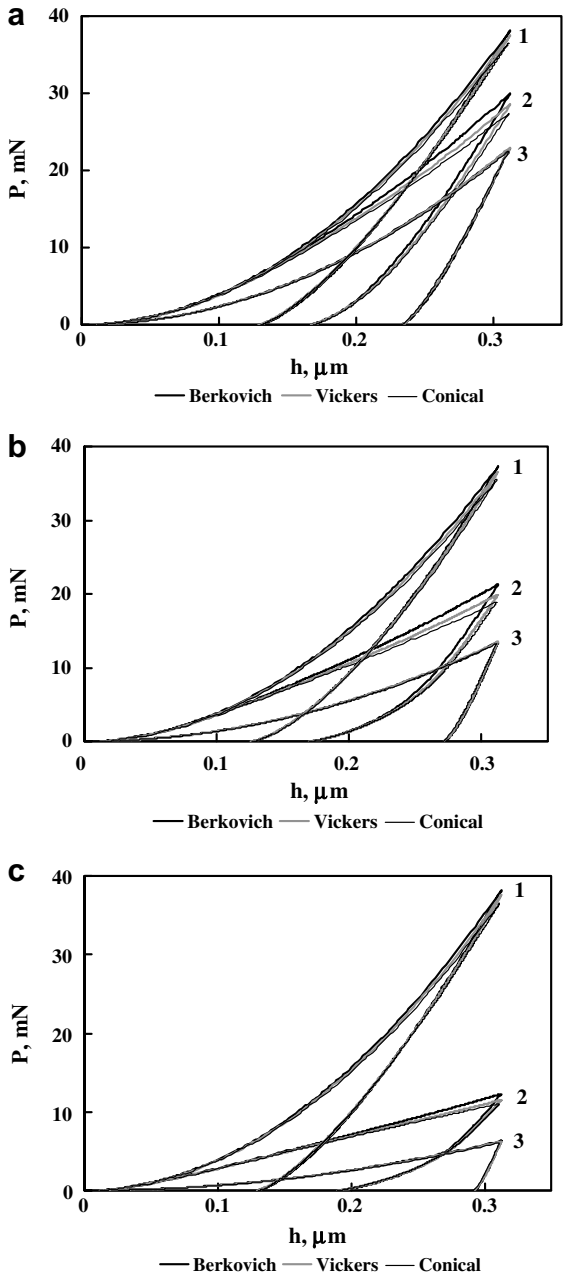

Fig. 8. Load–indentation depth curves for the composites: (a) C2 ($H_f^b/H_s^b = 2.22$); (b) C4 ($H_f^b/H_s^b = 4.33$); (c) C3 (($H_f^b/H_s^b = 8.67$)). Materials: 1, film; 2, composite; 3, substrate.

4.3. Friction coefficient

Finally, in order to check the influence of the friction coefficient value in the contact between the indented materials and the different indenter geometries, numerical simulations with friction coefficients of 0.04 and 0.30 were also carried out for both bulk and composite materials. Fig. 12 shows examples of load–indentation depth curves, corresponding to the B19 bulk material (Fig. 12(a)) and the C4 composite material (Fig. 12(b)), obtained with friction coefficients of 0.04, 0.16 and 0.30, for the cases of the Vickers and Berkovich indenter geometry. For all cases of bulk and composite materials studied, such as for the examples shown in Fig. 12, no measurable differences were observed in the load–indentation depth curves obtained with each indenter's geometry, whatever the value of the friction coefficient. This is in agreement

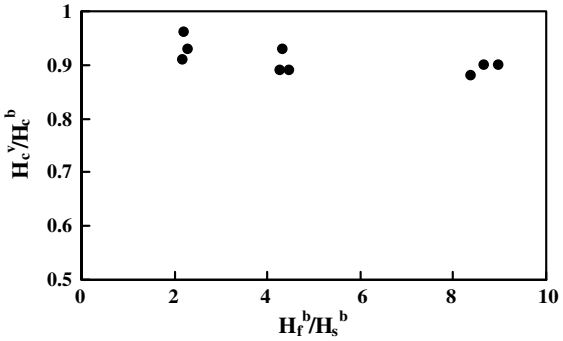

Fig. 9. Evolution of the ratio H_c^v/H_c^b, between the Vickers and the Berkovich hardness of the composite, of as function of the ratio H_f^b/H_s^b, between the Berkovich hardness of the film and the substrate.

with previous results on bulk materials which show that the Vickers hardness values are independent of the value of the friction coefficient used in the simulations (Antunes et al., 2006).

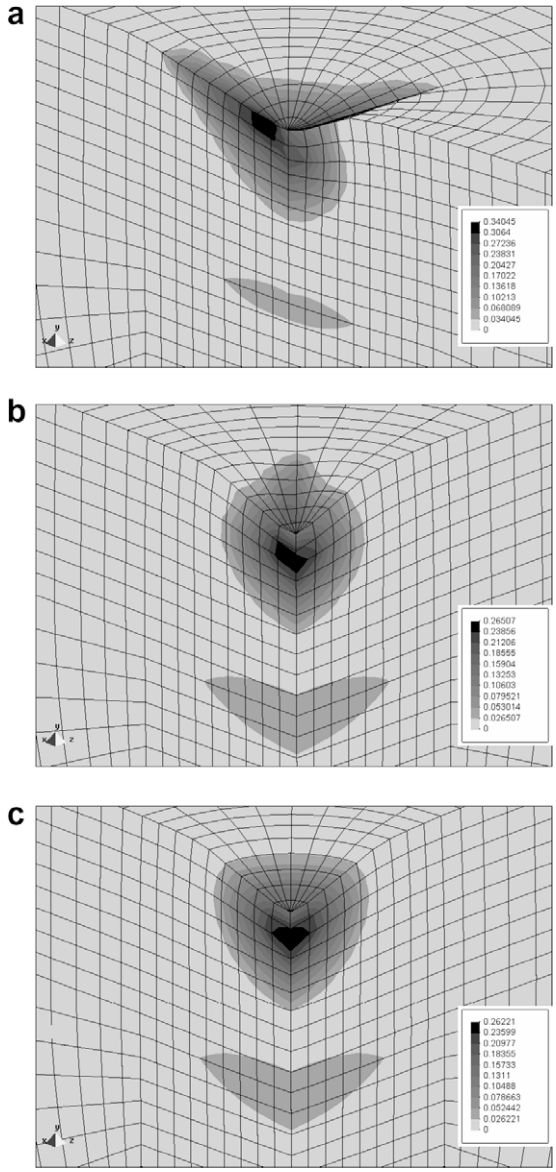

Fig. 10. Equivalent plastic strain distribution, at the penetration depth $h \approx 0.15$ μm, obtained in numerical simulation of the composite C2 ($H_f^b/H_s^b = 2.22$) for the indenters: (a) Berkovich; (b) Vickers; (c) conical.

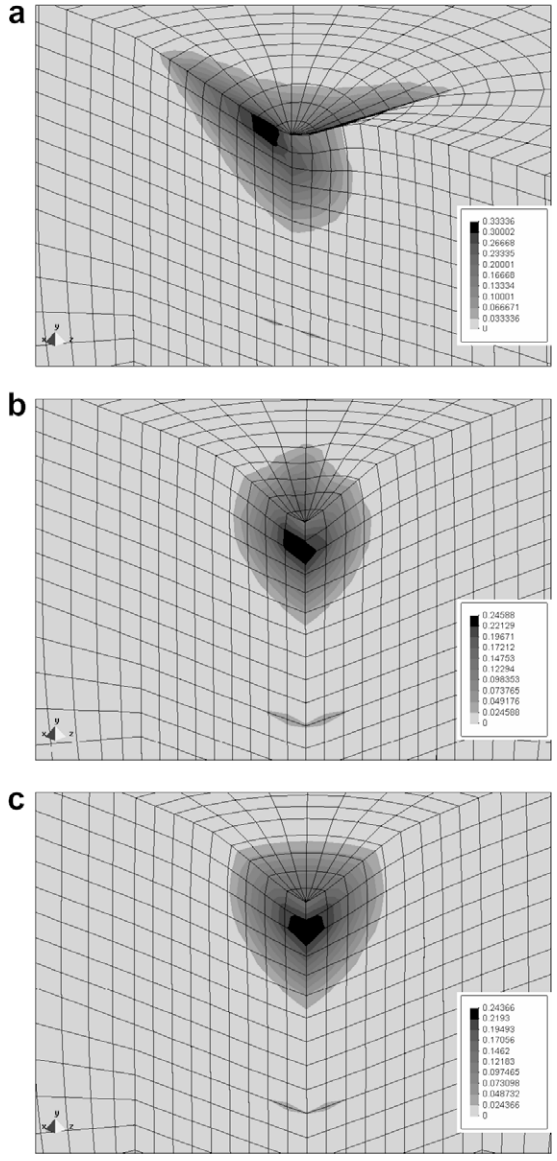

Fig. 11. Equivalent plastic strain distribution, at the initial stages of substrate plastic deformation, obtained in numerical simulation of the composite C2 ($H_f^b/H_s^b = 2.22$) for the indenters: (a) Berkovich ($h \approx 0.137$ μm); (b) Vickers ($h \approx 0.129$ μm); (c) conical ($h \approx 0.127$ μm).

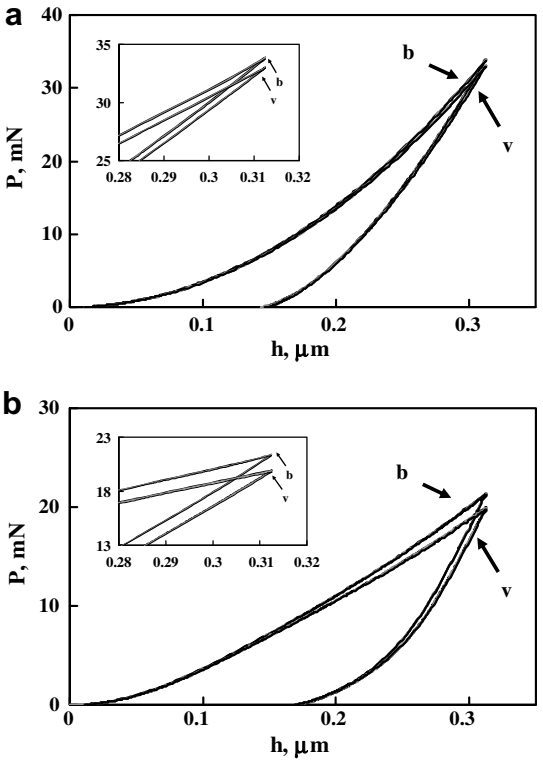

Fig. 12. Load–indentation depth curves obtained with the friction coefficients equal to 0.30, 0.16 and 0.04 for: (a) the bulk material B19; (b) the composite C4. Indenters: b, Berkovich; v, Vickers.

It can be concluded that the bulk and composite load–indentation depth responses to the hardness tests are independent of the friction coefficient (0.04, 0.16 or 0.30), whatever the indenter used, i.e., the load–indentation depth responses are not sensitive to the value of the friction coefficient (at least in the studied range). Thus, even if the friction coefficient value of 0.16, used in the simulations of previous sections, does not exactly correspond to the experimental one, the conclusions concerning the sensitivity of the load–indentation depth response to the indenter type, are still valid.

5. Conclusions

Three-dimensional numerical simulations of Berkovich, Vickers and conical indentation tests were performed in order to attain better understanding of the influence of the geometry of *equivalent* indenters on the materials' behaviour under indentation. The main following conclusions can be drawn:

- For bulk materials, covering a wide range of mechanical properties, the load–indentation depth curves obtained using the three indenters are difficult to distinguish, in cases of materials with high values of the h_f/h_{max} ratio (typically for $h_f/h_{max} > 0.65$) but can be separated for lower values of h_f/h_{max}. Therefore, the hardness values obtained show the same kind of behaviour. When comparing the results of the three indenters, the obtained levels for load–indentation depth curves and hardness are highest for the Berkovich and lowest for the conical. The results for the Vickers indenter lie between the two others, being closer to those for the conical indenter. Concerning the hardness, for the $h_f/h_{max} = 0$ ratio (purely elastic behaviour), the H^v/H^b and H^c/H^b ratios tend towards the values 0.947 and 0.923, respectively; and when the ratio $h_f/h_{max} = 1$ (rigid-plastic behaviour), both ratios H^v/H^b and H^c/H^b tend towards a value close to 1. This means that, when comparing Berkovich or Vickers experimental results or when replacing Berkovich or Vickers indenters with the conical one, in order to simplify numerical simulations, it is necessary to be cautious. For materials with low values of the h_f/h_{max} ratio, the equivalence between conical and Vickers indenters is closer than between conical and Berkovich indenters (or between Vickers and Berkovich indenters). For materials with high values of the h_f/h_{max} ratio, which corresponds in general to low to medium hardness, the equivalence between the three indenters can be considered acceptable.
- Some details of the equivalent plastic strain distributions are dependent on indenter geometry. In the case of bulk materials, the maximum value of equivalent plastic strain is higher for the Berkovich indenter than for the Vickers and conical ones, but the differences are attenuated for low values of h_f/h_{max}. This fact indicates that the increasing separation

between the load–indentation depth curves with decreasing h_f/h_{max} value is not related to differences in the maximum plastic strain values. The main possible reason for such behaviour is the differences in the geometry of the plastic strain regions obtained with the three types of indenter. The equivalent plastic strain distribution is less spherical and slightly less deep, for the Berkovich indenter than for the Vickers and conical ones for all materials, but mainly for the materials with low values of h_f/h_{max}.

- The results for composite materials where the ratio between the film (H_f) and the substrate (H_s) hardness's, H_f/H_s is higher than 2, show important distinctions in the function of the indenter geometry. The differences of the load–indentation depth curves and of hardness under Berkovich, Vickers and conical indenters are greater than for bulk materials, and depend on the H_f/H_s ratio. However, qualitatively, the relative position of the load–indentation depth curves and hardness values is similar to the case of bulk materials. It is shown that the substrate's contribution to the composite plastic deformation starts later (i.e., for higher penetration depth) and is less important in the case of Berkovich indentation than for Vickers and conical indentation. This is certainly the most important reason for the amplification of the differences between the responses under the three indenters for composite materials, when compared to bulk materials (knowing that for the studied composites the film is harder than the substrate). So, in the case of composites, one must be more cautious when comparing the hardness results of the three indenters. For example, the ratio between the Vickers and Berkovich hardnesses can attain 0.88, when the ratio between the hardness of the film and the substrate is 8.6.
- The bulk and composite load–indentation depth responses to the hardness tests are independent of the friction coefficient value (between 0.04 and 0.30), whatever the indenter used. So, even if the friction coefficient used in the numerical simulations does not exactly correspond to the experimental one, the conclusions concerning the sensitivity of the load–indentation depth response to the indenter type, are still valid.

Acknowledgements

The authors are grateful to the Portuguese Foundation for Science and Technology (FCT) who financially supported this work, through the Program POCTI (Portuguese Government and FEDER). One of the authors, N.A. Sakharova, was supported by a grant for scientific research from the Portuguese Science and Technology Foundation. This support is gratefully acknowledged.

References

Antunes, J.M., Cavaleiro, A., Menezes, L.F., Simões, M.I., Fernandes, J.V., 2002. Ultra-microhardness testing procedure with Vickers indenter. Surface and Coatings Technology 149, 27–35.

Antunes, J.M., Menezes, L.F., Fernandes, J.V., 2006. Three-dimensional numerical simulation of Vickers indentation tests. International Journal of Solids and Structures 43, 784–806.

Antunes, J.M., Menezes, L.F., Fernandes, J.V., 2007. Influence of Vickers tip imperfection on depth sensing indentation tests. International Journal of Solids and Structures 44, 2732–2747.

Bolshakov, A., Pharr, G.M., 1998. Influences of pileup on the measurement of mechanical properties by load and depth sensing indentation techniques. Journal of Materials Research 13 (4), 1049–1058.

Cheng, Y.-T., Cheng, C.-M., 1999. Scaling relationships in conical indentation of elastic perfectly plastic solids. International Journal of Solids and Structures 36 (8), 1231–1243.

Dao, M., Chollacoop, N., Van Vliet, K.J., Venkatesh, T.A., Suresh, S., 2001. Computational modelling of the forward and reverse problems in instrumented sharp indentation. Acta Materialia 49 (19), 3899–3918.

Joslin, D.L., Oliver, W.C., 1990. New method for analysing data from continuous depth-sensing microindentation tests. Journal of Materials Research 5 (1), 123–126.

Menezes, L.F., Teodosiu, C., 2000. Three-dimensional numerical simulation of the deep-drawing process using solid finite elements. Journal of Materials Processing Technology 97 (1–3), 100–106.

Min, Li, Wei-min, C., Nai-gang, L., Ling-dong, W., 2004. A numerical study of indentation using indenters of different geometry. Journal of Materials Research 19, 73–78.

Oliveira, M.C., 2006. Algorithms and Strategies for the Treatment of Large Deformation Frictional Contact Mechanics – Application to sheet metal forming. Ph.D. Thesis, University of Coimbra, Portugal.

Oliveira, M.C., Alves, J.L., Menezes, L.F., 2008. Algorithms and strategies for treatment of large deformation frictional contact in the numerical simulation of deep drawing process. Archives of Computational Methods in Engineering 15, 113–162.

Oliver, W.C., Pharr, G.M., 1992. An improved technique for determining hardness and elastic-modulus using load and displacement sensing indentation experiments. Journal of Materials Research 7 (6), 1564–1583.

Rother, B., Steiner, A., Dietrich, D.A., Jehn, H.A., Haupt, J., Giessler, W., 1998. Depth-sensing indentation measurements with Vickers and Berkovich indenters. Journal of Materials Research 13 (8), 2071–2076.

Sneddon, I.N., 1965. The relation between load and penetration in the axisymmetric Boussinesq problem for a punch of arbitrary profile. International Journal of Engineering Science 3, 47–56.

Tanner J.A., 1996. Computational Methods for Frictional Contact with Applications to the Space Shuttle Orbiter Nose-Gear Tire – Development of Frictional Contact Algorithm. NASA Technical Paper 3574, pp. 48.